Available online at www.sciencedirect.com
SCIENCE DIRECT
Journal of Organometallic Chemistry 691 (2006) 799–804
Journal of Organometallic Chemistry
www.elsevier.com/locate/jorganchem

Syntheses and structures of new luminescent B(III) complexes: BPh_2(2-(2-pyridyl)naphtho[b]imidazole) and BF_2(2-(2-pyridyl)naphtho[b]imidazole)

Tsun-Ren Chen [a,*], Rong-Hong Chien [b], Ming-Shiun Jan [b], Anchi Yeh [*,b], Jhy-Der Chen [*,c]

[a] Department of Electrical Engineering, Yung-Ta Institute of Technology, Ping-Tung, Taiwan, ROC
[b] Department of Chemical Engineering, Chengshiu University, Kaohsiung, Taiwan, ROC
[c] Department of Chemistry, Chung-Yuan Christian University, Chung-Li, Taiwan, ROC

Received 21 September 2005; received in revised form 16 October 2005; accepted 16 October 2005
Available online 28 November 2005

Abstract

A novel chelating ligand, 2-(2-pyridyl)naphtho[b]imidazole (PNI) has been synthesized and structurally characterized. The PNI molecule reacts readily with BPh_3 and BF_3 to form BPh_2(2-(2-pyridyl)naphtho[b]imidazole) (**1**) and BF_2(2-(2-pyridyl)naphtho[b]imidazole) (**2**), respectively. The structures of PNI and **1** were determined by single crystal X-ray diffraction, while that **2** by spectroscopic methods. The structure of **1** reveals that the boron center is four-coordinated. The electroluminescent device using **1** as the emitting layer shows bright yellow luminescence with a maximum emission peak at 540 nm. Complexes **1** and **2** form a new family of organometallic emitting materials which could be of interest for practical applications.

Keywords: Electroluminescence; Imidazole; Boron; Intramolecular charge transfer (ICT)

1. Introduction

The chemistry of organoboron complexes have attracted much more attention recently because they are of interest for practical applications [1–3]. Since an organic light emitting diode (OLED) was reported by Tang and Vanslyke [4], LEDs based on organic materials have generated considerable interest and enabled the development of low-cost, full-color, flat-panel displays [5–8]. The best-known EL metal complex used in OLED is Alq_3 which is not only a good emitter but also a highly efficient electron-transporting material, where q is the 8-hydroxyquinolinato ligand [9,10]. Via the modification of the ligand of metal complex, the emission spectra of devices and other properties, such as thermostability and carrier mobility, can be tuned. Most of imidazoles are good chelating ligands and can force the resultant metal complexes into special geometries [11], and the attachment of the pyridyl group at 2-position of imidazoles would allow the ligands to form the stable complexes with metals. Therefore, the imidazole ligands containing pyridyl group (PNI) were prepared in this work, and the complexes, BPh_2(2-(2-pyridyl)naphtho[b]imidazole) (**1**) and BF_2(2-(2-pyridyl)naphtho[b]imidazole) (**2**), have been synthesized for the first time. The details of syntheses, structures, and luminescent properties of those boron complexes are reported.

2. Results and discussion

2.1. Syntheses and characterization

2.1.1. The PNI ligand

The synthesis of PNI was carried out using a modified literature method reported previously for related compounds

* Corresponding author. Tel./fax: +886 8 7333632.
E-mail addresses: trchen@mail.ytit.edu.tw, lspccj@ms14.hinet.net (T.-R. Chen).

0022-328X/$ - see front matter © 2005 Elsevier B.V. All rights reserved.
doi:10.1016/j.jorganchem.2005.10.022

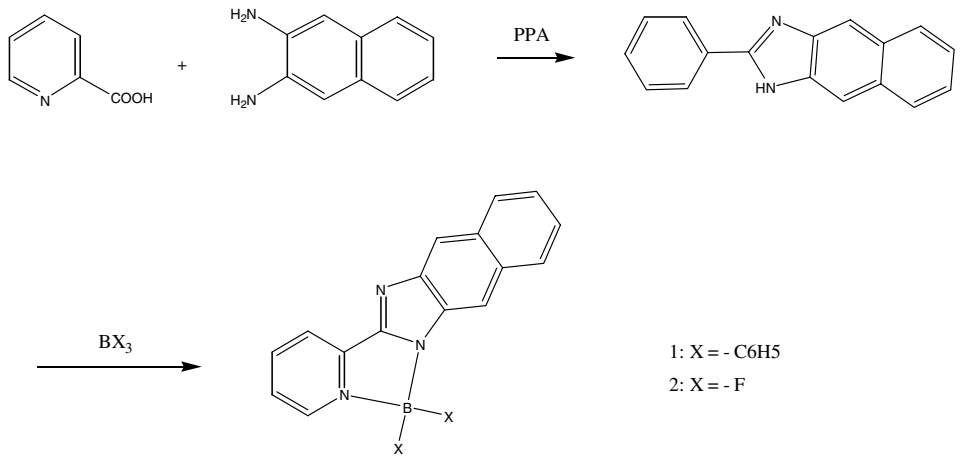

Scheme 1.

[12,13] in high yield (Scheme 1). The structure of PNI was determined by single-crystal X-ray diffraction analysis. Fig. 1 shows an ORTEP diagram of PNI. The dihedral angle between imidazol moiety and quinoline ring, 8°, reveals that this molecule approximates to a plane structure stabilized by an intramolecular hydrogen bonding, N(1)–H···N(3) (2.578 Å). The C(5)–C(6) bond length of 1.464(10) Å is shorter than a single bond length, indicative of the conjugation of the imidazol moiety and quinoline ring, which also show that the plane structure is stabilized by the delocalization of π-electrons of the heterocyclic system.

2.1.2. The complexes of 1 and 2

Complexes **1** and **2** were prepared by reacting PNI with appropriate boron compounds in dry THF (Scheme 1). Both the complexes are air-stable in the solid state and in solution. The thermogravimetric analysis (TGA) scans under nitrogen for **1** and **2** powders showed weight loss of 10% at 337 and 310 °C, respectively, which reveal that both of **1** and **2** are quite stable in the atmosphere of nitrogen. The DSC showed the melting point of complexes **1** and **2** were 276 and 250 °C, respectively, which may serve as an advantage for OLED device fabrication because the materials having high melting point could provide the device with greater longevity [14,15].

2.1.3. Structure of 1

Single crystals of **1** were grown by slow diffusion of hexane into a concentrated solution of complex **1** in dichloromethane. The molecular structure of **1** is shown in Fig. 2 and the selected bond lengths and angles are listed in Table 1. In this structure, the boron atom in **1** has a typical tetrahedral geometry. The PNI ligand is bidentately chelated to the boron center through its pyridyl and imidazole nitrogen atoms and two phenyl groups occupy the other boron sites. The bond length of B–N(2) imidazole bond (1.558(4) Å) is shorter than that of the B–N(1) pyridyl bond (1.624(4) Å), indicating that the imidazole nitrogen is anionic and hence a better donor than the neutral

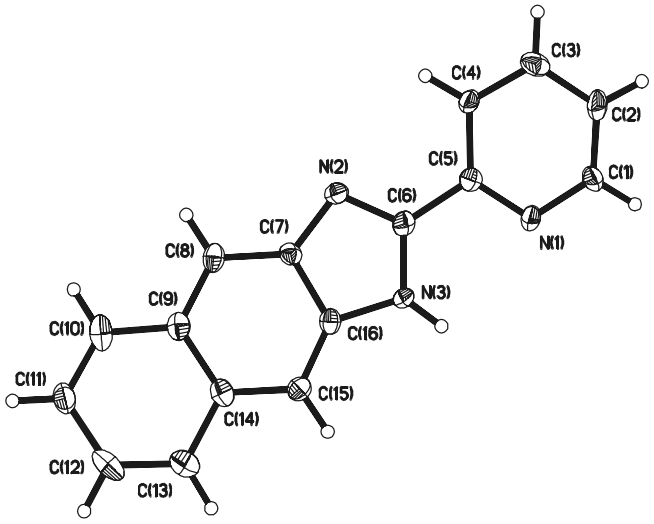

Fig. 1. An ORTEP drawing of the molecular structure of PNI with 20% thermal and labeling schemes.

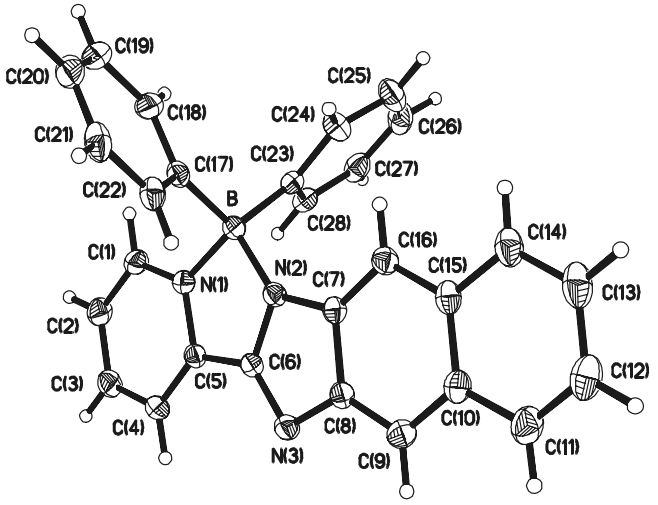

Fig. 2. An ORTEP drawing of the molecular structure of complex **1** with 20% thermal and labeling schemes.

Table 1
Selected bond distance (Å) and angles (°)

PNI			
Bond lengths		*Bond angles*	
N(1)–C(5)	1.325(8)	C(5)–N(1)–C(1)	116.2(6)
N(1)–C(1)	1.353(8)	C(6)–N(2)–C(7)	103.3(5)
N(2)–C(6)	1.349(8)	C(6)–N(3)–C(16)	107.7(5)
N(2)–C(7)	1.384(8)	C(2)–C(1)–N(1)	124.1(6)
N(3)–C(6)	1.350(8)	N(1)–C(5)–C(4)	123.7(6)
N(3)–C(16)	1.407(8)	N(1)–C(5)–C(6)	115.4(7)
C(4)–C(5)	1.410(9)	C(4)–C(5)–C(6)	120.9(7)
C(5)–C(6)	1.464(10)	N(2)–C(6)–C(5)	123.2(7)
C(7)–C(8)	1.406(8)	N(3)–C(6)–C(5)	123.0(7)
1			
Bond angles		*Bond angles*	
N(1)–C(1)	1.339(4)	C(1)–N(1)–C(5)	119.5(3)
N(1)–C(5)	1.359(4)	C(5)–N(1)–B	113.1(2)
N(1)–B	1.624(4)	C(6)–N(2)–B	113.8(2)
N(2)–C(6)	1.361(4)	C(6)–N(3)–C(8)	101.9(2)
N(2)–C(7)	1.385(4)	N(2)–B–C(23)	111.1(3)
N(2)–B	1.558(4)	N(2)–B–N(1)	94.8(2)
N(3)–C(6)	1.316(4)	C(23)–B–N(1)	111.6(3)
N(3)–C(8)	1.398(4)	C(1)–N(1)–B	127.5(3)
C(17)–B	1.607(5)	C(6)–N(2)–C(7)	104.3(2)
C(23)–B	1.611(5)	C(7)–N(2)–B	141.7(3)
		N(2)–B–C(17)	114.2(3)
		C(17)–B–C(23)	114.5(3)
		C(17)–B–N(1)	109.0(2)

pyridyl nitrogen atom [2]. The two five-membered rings are nearly coplanar with a dihedral angle of 2.6° between these two rings. Fig. 3 shows a packing diagram for **1**. The interplanar distances between imidazol moiety and pyridyl ring are in the range of 3.4–3.8 Å, which implies that the interlayer π–π interaction may play an important role in producing bathochromic shift of absorption maximum in solid state and red shift of PL spectra in higher concentration in solution [16].

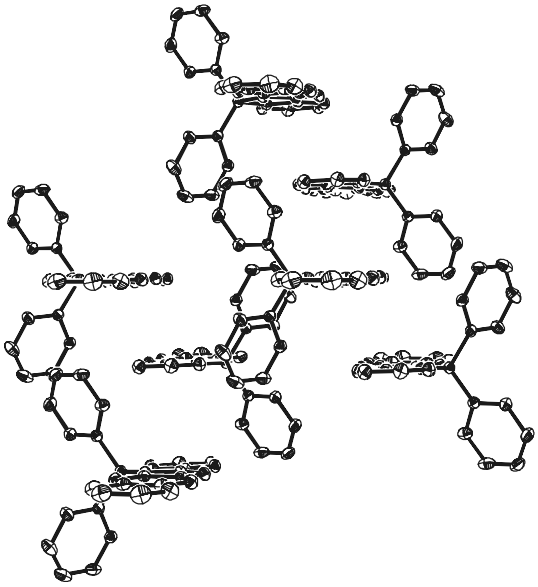

Fig. 3. An illustration of the stacking present in crystal **1**.

2.1.4. Electronic absorption and photoluminescence spectra

At room temperature and low concentration (1×10^{-5} M), the absorption spectrum of PNI in dichloromethane consist of two discrete bands (Fig. 4). A strong absorption which can be assigned to the π–π* transition centered at 282 nm. The other intense band centered at 344 nm shows a vibrational separation of 1300 cm^{-1} with the $v_{0,0}$ transition at 3.03×10^4 cm^{-1}. This lower energy band possesses a reasonably high absorptivity ($\varepsilon \sim 10^4$ dm^3 mol^{-1} cm^{-1}) and a bathochromic shift with increasing polarity of solvent, which are consistent with the intramolecular charge transfer (ICT) character for the concerned π–π* transition involving the filled π orbital (HOMO) located on the imidazol ring and the unoccupied π* orbital (LUMO) located on the quinoly ring [17–23]. For the absorption spectrum of **1** (Fig. 4), based on the comparisons with the spectrum of PNI, we attribute the bands at 372, and 278 nm to metal-perturbed ligand-localized (LC) transition. Interestingly, the BPh_2 group lowers the π → π* energy gap of PNI, which could be attributed to the fact that the π system of molecule is more extensive when the BPh_2 group bonds to PNI, resulting in the decrease of the HOMO–LUMO energy gap. For the absorption spectrum of **2**, the bands at 267, and 345 nm are also attributed to LC transition, which is similar to that of PNI, indicating that the BF_2 group can hardly affect the π system of PNI.

Fig. 5 shows the photoluminescence (PL) spectra of **1** in various concentrations, excited with 355 nm laser line. At low concentration, 1×10^{-8} M in DMF, only one emission band was observed with a maximum at 413 nm, which corresponds to the relaxation of **1** from the excited state of a single molecule into ground state. Interestingly, when the concentration was increased to 1×10^{-7} M, a new emission band having a maximum at 550 nm was observed, which can be attributed to the formation of excimers by exciting monomers that happened to be in ground-state [24–27]. When the solution became more concentrated, reaching 1×10^{-4} M, the monomer emission disappeared and only the excimer emission existed.

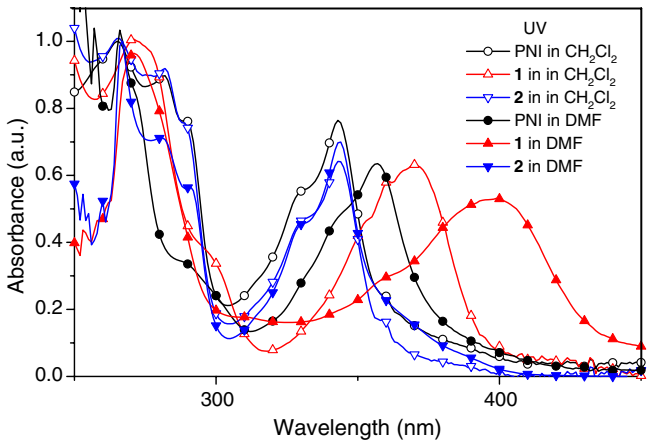

Fig. 4. UV–vis spectra of PNI, **1** and **2** in *N*,*N*′-dimethylformamide and dichloromethane.

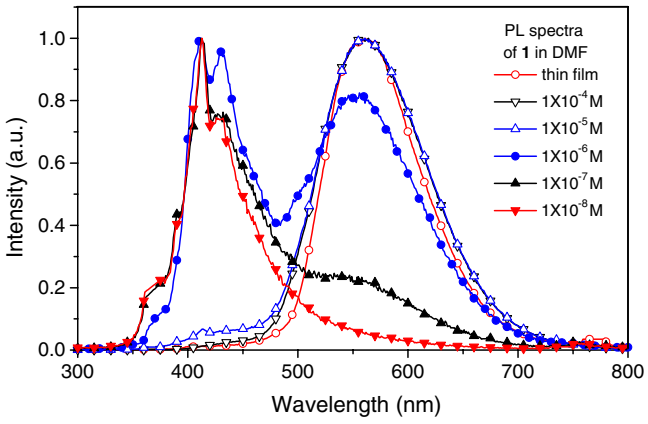

Fig. 5. Photoluminescence spectra of complex **1** in various concentrations, excited with 355 nm laser line.

The photoluminescence (PL) spectra of the solutions of **2**, excited with 355 nm laser line, are illustrated in Fig. 6. Both at low concentration and at high concentration, only one emission band was observed with a maximum at 435 nm, which corresponds to the relaxation of **2** from the excited state of a single molecule into ground state. The excimer emission was not observed for **2**.

The complexes **1** and **2** possess the appreciable PL quantum yields, $\Phi_f = 0.8$ and 0.2, respectively, in DMF relative to 3-(2-benzothiazolyl)-7-diethyl-aminocoumarin (C540).

2.1.5. Electroluminescence study

In order to evaluate the electroluminescence characteristic of PNI–boron complex, a three-layer OLED having the configuration of ITO/NPB (50 nm)/**1** (50 nm)/Alq_3 (50 nm)/MgAg (100 nm) was fabricated, in which *N*,*N*′-bis-(1-naphthyl)-*N*,*N*′-diphenyl-1,1′-biphenyl-4,4′-diamine (NPB) was used as a hole-transport material (HTM), the complex **1** was used as an emitter, and tris(8-quinnolinolato) aluminum (Alq_3) was employed as an electron-transporting material (ETM). The organic layers and the cathode were sequentially deposited by conventional vacuum-vapor deposition in the same chamber without breaking the vacuum under 3×10^{-6} Torr. Before the deposition, all of the organic materials were purified by a train sublimation method. The thickness of the organic layers and cathode were measured by quartz-crystal monitor.

This device possesses a yellow emission (CIE coordinates $x = 0.45$ and $y = 0.53$) and the EL peak at 543 nm, Fig. 7. Though the pattern of EL spectrum of this device is similar to that of PL spectrum of **1** in higher concentration, the EL peak is shifted about 20 nm, which could be attributed to the interaction occurring at the interface between emitting layer and ETM. The voltage–current density and luminance–voltage characteristics of this device, Fig. 8, shows that the turn-on voltage is 3.5 V with a maximum luminance of 332 cd/m^2 at 10 V and a maximum luminance efficiency of 0.02 lm/W at 7 V.

In conclusion, we have demonstrated that the novel PNI ligand is capable of chelating to B(III) center and the resulting complexes possess appreciable photoluminescent efficiency and have a very high thermal stability, which are important characters for practical application in the electronic fields, especially for OLED.

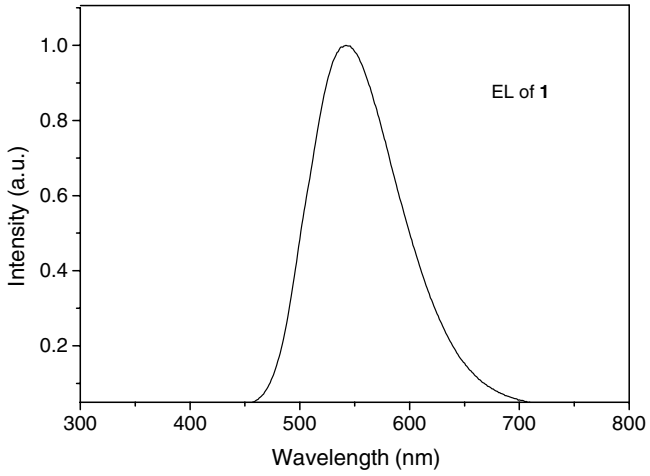

Fig. 7. Electroluminescence spectrum of the EL device.

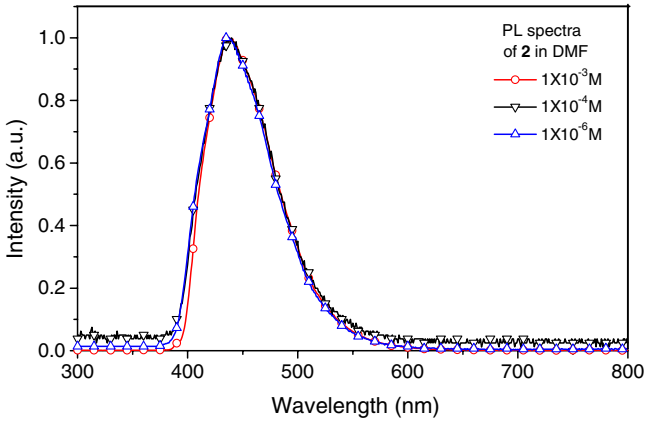

Fig. 6. Photoluminescence spectra of complex **2** in various concentrations, excited with 355 nm laser line.

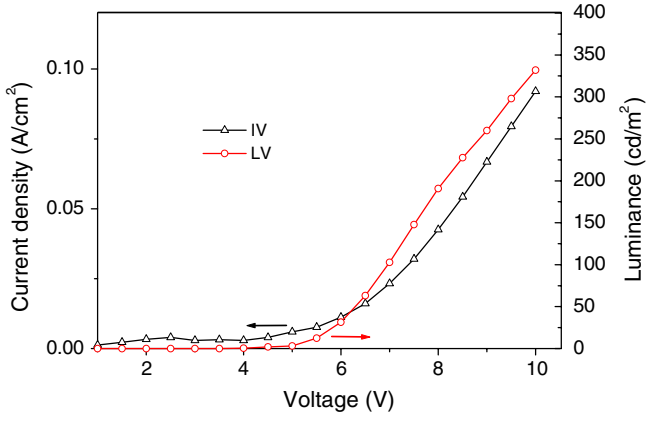

Fig. 8. Current–voltage and luminance–voltage characteristics of the EL device.

3. Experimental

3.1. General procedure

All starting materials were purchased from Aldrich Chemical Co. ^{1}H and ^{13}C NMR spectra were recorded on the Bruker 300 MHz NMR spectrometers in $CDCl_3$. Thermogravimetric analyses (TGA) were performed on a Perkin–Elmer thermogravimeter (Pyris 1) under a dry nitrogen gas flow at the heating rate of 20 °C/min. Glass transition temperature (T_g) and melting point (T_m) of materials were determined by differential scanning calorimeter (DSC) of the Perkin–Elmer differential scanning calorimeter (DSC-7). The absorption spectra were recorded with the HP-8453A UV–vis photodiode array spectrophotometer. The EL spectrum and the Commission Internationale de I'Eclairage (CIE) co-ordinates were measured by Pro-650 Spectroscanner, the current–voltage (I–V) characteristics were measured by Keithley 2400 Source meter. Photoluminescence (PL) was measured by Model LS 55 luminescence Spectrometer.

3.2. Synthesis of 2-(2-pyridyl)naphtho[b]imidazole (PNI)

Pyridine-2-carboxylic acid (20.0 mmol, 2.46 g), 2,3-diaminonaphthalene (20.0 mmol, 3.16 g), and polyphosphoric acid (PPA, 20 ml) were added to a flask. The mixture was heated at 200 °C for 4 h. After cooling to room T, the residue was slowly added to deionized water (500 ml) with stirring. The solid was collected by suction filtration and purified by column chromatography. Colorless crystals of PNI were obtained in 80% yield. M.p. >250 °C. ^{1}H NMR (500 MHz, DMF-d^7, 293 K), δ ppm: 13.3 (s, 1H, NH), 8.83 (d, 1H, $J = 4$ Hz, pyridyl), 8.58 (d, 1H, $J = 7.8$ Hz, pyridyl), 8.40 (s, 1H, imidazole), 8.21 (s, 1H, imidazole), 8.13 (dd, 2H, $J = 7.7$, 1.7 Hz, imidazole), 8.07 (t, 1H, $J = 10$, 1.2 Hz, pyridyl), 7.62 (m, 1H, imidazole), 7.45 (m, 2H, pyridyl). Anal. Calc. for $C_{16}H_{11}N_3$ (MW = 245.28): C, 78.36; H, 4.48; N, 17.14. Found: C, 78.31; H, 4.50; N, 17.11%.

3.3. Syntheses of 1 and 2

Complexes **1** and **2** were prepared in dry THF by reacting, in a 1:1.05 molar ratio, PNI with triphenylboron or boron trifluoride. The solutions were refluxed for 12 h under nitrogen. Selected analytical data concerning **1** and **2** are:

3.4. BPh_2(2-(2-pyridyl)naphtho[b]imidazole) (1)

Pale yellow solid. 35% yield. M.p. > 250 °C. ^{1}H NMR (500 MHz, DMF-d^7, 293 K), δ ppm: 8.67 (d, 1H, $J = 13$ Hz, pyridyl), 8.63 (d, 1H, $J = 13.5$ Hz, pyridyl), 8.40 (s, 1H, imidazole), 8.29 (t, 1H, $J = 15$, 2 Hz, pyridyl), 8.0 (dd, 1H, $J = 13$, 1.2 Hz, pyridyl), 7.84 (s, 1H, imidazole), 7.81 (d, 1H, 7.5 Hz, pyridyl), 7.65 (m, 1H, imidazole), 7.33 (m, 6H, ph and imidazole), 7.27 (m, 7H, ph and imidazole). MS data: 409.29 (26.643%), 332.2 (100%), 295.2 (11.59%), 245.2 (19.26%), 239.2 (19.37%), 166.1 (9.77%), 91.1 (6.69%). Anal. Calc. for $C_{28}H_{20}N_3B$ (MW = 409.2): C, 82.11; H, 4.88; N, 10.26. Found: C, 82.09; H, 4.93; N, 10.24%.

3.5. BF_2(2-(2-pyridyl)naphtho[b]imidazole) (2)

Pale yellow solid. 30% yield. M.p. > 250 °C. ^{1}H NMR (500 MHz, DMF-d^7, 293 K), δ ppm: 8.69 (d, 1H, $J = 6.3$ Hz, pyridyl), 8.56 (d, 1H, $J = 7.8$ Hz, pyridyl), 8.11 (s, 2H, imidazole), 7.95 (m, 3H, pyridyl and imidazole), 7.43 (m, 3H, imidazole and imidazole). Anal. Calc. for $C_{16}H_{10}N_3BF_2$ (MW = 293.09): C, 65.57; H, 3.44; N, 14.34. Found: C, 65.53; H, 3.50; N, 14.30%.

3.6. Determination of the crystal structure

The diffraction data of PNI and complex **1** were collected on a Bruker AXS P4 diffractometer, which is equipped with graphite-monochromated Mo Kα radiation ($\lambda = 0.71073$ Å). Structure refinements were carried out using the SHELXTL software package [28]. The structure factors were obtained after Lorentz and polarization corrections. The positions of some of the heavier atoms were located by the direct method. The remaining atoms were found in a series of alternating difference Fourier maps

Table 2
Crystal data and structure refinement parameters

Compound	PNI	**1**
Empirical formula	$C_{16}H_{11}N_3$	$C_{28}H_{20}B\ N_3$
Formula weight	245.28	409.2
Crystal system	Orthorhombic	Triclinic
Space group	$P2(1)2(1)2(1)$	$P\bar{1}$
Unit cell dimensions		
a (Å)	10.866(2)	9.2216(8)
b (Å)	14.3173(17)	9.6733(16)
c (Å)	23.011(2)	15.2655(17)
α (°)	90	97.220(10)
β (°)	90	90.921(8)
γ (°)	90	115.787(8)
Volume (Å^3)	3579.7(9)	1212.6(3)
Z	12	2
Calculated density (Mg m^{-3})	1.365	1.237
Absorption coefficient (mm^{-1})	0.084	0.179
$F(000)$	1536	470
Crystal size (mm)	$0.2 \times 0.5 \times 0.3$	$0.2 \times 0.6 \times 0.4$
θ Range for data collection (°)	1.77–24.99	2.36–25.00
Reflections collected	4394	5039
Data/restraints/parameters	4177/0/515	4200/0/317
Goodness-of-fit on F^{-2}	1.054	1.134
Final R indices [$I > 2$sigma(I)]	$R1 = 0.0647$	$R_1 = 0.0783$
	$wR2 = 0.1471$	$wR_2 = 0.2017$
R indices (all data)	$R1 = 0.1263$	$R1 = 0.1125$
	$wR2 = 0.1838$	$wR2 = 0.2266$
Largest difference peak and hole (e Å^{-3})	0.320 and −0.353	0.725 and −0.362

$R_1 = \sum\|F_o| - |F_c\|/\sum F_o|$; $wR_2 = [\sum w(F_o^2 - F_c^2)^2/\sum w(F_o^2)^2]^{1/2}$; quality-of-fit $= [\sum w(|F_o^2| - |F_c^2|)^2/N_{\text{observed}} - N_{\text{parameters}}]^{1/2}$; $w = 1/[\sigma^2(F_o^2) + (\text{ap})^2 + (\text{bp})]$; $p = [\max(F_o^2 \text{ or } 0) + 2(F_c^2)]/3$; $a = 0.0185$, $b = 25.8531$.

and least-square refinements. Selected bond distances and angles are listed in Table 1 and basic information pertaining to crystal parameters and structure refinement is summarized in Table 2.

4. Supplementary material

Crystallographic data for the structural analysis has been deposited with the Cambridge Crystallographic Data Centre as supplementary publication numbers CCDC 283102. Copies of the data can be obtained, free of charge, on application to CCDC, 12 Union Road, Cambridge CB2 1EZ, UK [fax: +44 0 1223 336033 or e-mail: deposit@ccdc.cam.ac.uk].

Acknowledgement

We thank the National Science Council of ROC for financial support.

References

[1] D. Song, S.F. Liu, R.Y. Wang, S. Wang, J. Organomet. Chem. 631 (2001) 75.
[2] Q. Liu, M.S. Mudadu, H. Schmider, R. Thummel, Y. Tao, S. Wang, Organometallics 21 (2002) 4743.
[3] J.E. Lee, G.C. Choi, B.O. Rim, S.M. Kim, N.G. Park, Y.K. Ha, Y.S. Kim, Mater. Sci. Eng. C 24 (2004) 269.
[4] C.W. Tang, S.A. VanSlyke, Appl. Phys. Lett. 51 (1987) 913.
[5] C. Adachi, S. Tokito, J. Tsutusi, S. Saito, Jpn. J. Appl. Phys. 27 (1988) 713.
[6] J.H. Burroughes, D.D.C. Bradley, A.R. Brown, R.N. Marks, K. Mackay, R.H. Friend, P.L. Burns, A.B. Homes, Nature 347 (1990) 539.
[7] J.R. Sheats, H. Antoniadis, M. Hueschen, W. Leonard, J. Miller, R. Moon, D. Roitman, A. Stocking, Science 273 (1996) 884.
[8] H. Nakada, T. Tohma, Inorganic and Organic Electroluminescence, Wissenschaft-und-Technik-Verlag, Berlin, 1996, p. 385.
[9] S.-F. Liu, C. Seward, H. Aziz, N.-X. Hu, Z. Popovic, S. Wang, Organometallics 19 (2000) 5709.
[10] H. Schmidbaur, J. Lettenbauer, D.L. Wilkinson, G. Muller, O.Z. Kumberger, Naturforsch 46B (1991) 901.
[11] R. Balamurugan, M. Palaniandavar, Inorg. Chem. 40 (2001) 2246.
[12] T.R. Chen, J. Mol. Stuct. 737 (2005) 35.
[13] T.R. Chen, A. Yeh, J.D. Chen, Tetrahedron Lett. 46 (2005) 1569.
[14] Z.-K. Chen, H. Meng, Y.-H. Lai, W. Huang, Marcromolecules 32 (1999) 4351.
[15] S. Tokito, H. Tanaka, K. Noda, A. Okada, Y. Taga, Appl. Phys. Lett. 70 (1997) 1929.
[16] J.H. Kim, M. Matsuoka, K. Fukunishi, Dyes Pigments 40 (1998) 53.
[17] F. Peral, E. Gallego, J. Mol. Struct. 372 (1995) 101.
[18] A. Sarkar, S. Chakravorti, J. Lumin. 65 (1995) 163.
[19] Y.V. Ilichev, W. Kuhnle, K.A. Zachariasse, J. Chem. Phys. 211 (1996) 441.
[20] A.-A. Ibrahim, Bull. Soc. Chim. Fr. 134 (1997) 593.
[21] M. La Deda, M. Ghedini, I. Aiello, T. Pugliese, F. Barigelletti, G. Accorsi, J. Organomet. Chem. 690 (2005) 857.
[22] I. Aiello, M. Ghedini, M. La Deda, J. Lumin. 96 (2002) 249.
[23] N.G. Park, J.E. Lee, Y.H. Park, Y.S. Kim, Synth. Met. 145 (2004) 279.
[24] R. Aroca, T.D. Cano, Chem. Mater. 15 (2003) 38.
[25] H. Beens, A. Weller, in: J.B. Birks (Ed.), Organic Molecular Photophysics, vol. 2, Wiley, New York, 1975, p. 159.
[26] S. Santra, G. Krishnamoorrhy, S.K. Dogra, J. Mol. Stuct. 559 (2001) 25.
[27] S. Santra, Santra K. Dogra, J. Mol. Stuct. 476 (1999) 223.
[28] SHELXTL 5.10. Bruker Analytical X-ray Instruments Inc., Karlsruche, Germany, 1997.